Journal of
Materials Chemistry C

REVIEW

View Article Online
View Journal | View Issue

Cite this: J. Mater. Chem. C, 2018, 6, 2915

Energy level alignment of dipolar interface layer in organic and hybrid perovskite solar cells

Kyung-Geun Lim,[a] Soyeong Ahn[b] and Tae-Woo Lee *[c]

The dipole moment of interface materials has played the key role in efficient charge extraction in organic and hybrid perovskite solar cells, but the mechanisms of the interaction at the interface and of the resulting energy level alignment have not been well established. In this review, the decoupled dipole moments at the interface are investigated and clarified by using both the theoretical and experimental findings, with particular focus on dipolar interface materials and the consequent energy level alignment in organic and hybrid perovskite solar cells. The mechanisms of interface dipole moments in the interface layer are evaluated by using spontaneously and nonspontaneously aligned dipolar molecules, thereby the energy-level adjustment of the dipolar interface layer in the devices are elucidated. The diverse dipolar interface materials (*e.g.*, self-assembled monolayers, conjugated or nonconjugated polymer, neutral molecules or electrolytes, zwitterion based molecules, electrolyte grafted copolymer) are introduced and classified according to their working mechanisms of decoupled dipole moments at the interface. We conclude that an efficient interface material and its particular treatment can be designed and developed by exploring the underlying mechanisms of the decoupled dipole moments. Therefore, device characteristics may be advanced by the insights provided in this review.

Received 11th January 2018,
Accepted 26th February 2018

DOI: 10.1039/c8tc00166a

rsc.li/materials-c

[a] Korea Research Institute of Standards and Science (KRISS), 267 Gajeong-ro, Yuseong-Gu, Daejeon 34113, Republic of Korea. E-mail: kglim@kriss.re.kr
[b] Department of Materials Science and Engineering, Pohang University of Science and Technology (POSTECH), San 31 Hyoja-dong, Nam-gu, Pohang, Gyungbuk 790-784, Republic of Korea
[c] Department of Materials Science and Engineering, Research Institute of Advanced Materials, BK21 PLUS SNU Materials Division for Educating Creative Global Leaders, Seoul National University, 1 Gwanak-ro, Gwanak-gu, Seoul 08826, Republic of Korea. E-mail: twlees@snu.ac.kr, taewlees@gmail.com

Introduction

Newly-developed interface materials have contributed to a large increase in the power conversion efficiency (PCE) of organic solar cells and organic–inorganic hybrid perovskite solar cells. The interface materials have crucial functions in energy level alignment, charge transfer, trap passivation and operational stability of organic and perovskite solar cells.[1] Energy level

Kyung-Geun Lim

Kyung-Geun Lim is a senior research scientist at Korea Research Institute of Standards and Science (KRISS), Korea. He received PhD in the Department of Materials Science and Engineering from Pohang University of Science and Technology (POSTECH), Korea (2015). He joined Dresden Integrated Center for Applied Physics and Photonic Materials (IAPP), Germany as a postdoctoral researcher (2015–2017). He has been performing research on the flexible electronics based on organic and organic–inorganic hybrid materials for energy and transistor devices.

Soyeong Ahn

Soyeong Ahn is currently a PhD candidate in Materials Science and Engineering at Pohang University of Science and Technology (POSTECH), Korea. She received her MS and BS degrees in Chemical Engineering from Kyung Hee University in February 2015. Her current research focuses on solution-processed electronics based on organic and organic–inorganic hybrid materials for flexible displays, solid-state lightings, and solar energy devices.

alignment and the consequent device characteristics are critically affected in different ways by interface materials.[2–4]

For instance, the different adsorption types between a conjugated small molecule or polymer with its substrate can cause various effects on charge transfer and dipole moment. Examples include polarization by image charge (*i.e.*, one of interface dipoles), partial charge transfer *via* organic-substrate covalent bonds (*i.e.*, bond dipole), integer charge transfer (by the bipolaron state), surface rearrangement across the interface, and adsorption-induced molecular ordering.[2,3] Therefore, the interaction model can be classified according to interaction strength (*e.g.*, weak or strong), type of interface (*e.g.* noble metal atoms, hydrocarbons, conjugated molecules, or molecules with anchoring groups on substrate), or type of interaction (*e.g.*, physisorption, chemisorption, covalent bond).[3] The interaction type is also critically affected by processing conditions, such as vacuum pressure in the evaporation chamber during deposition.[5,6]

The dipole moment of the interface layer and the consequent energy level modification vary according to the conformations of dipolar interface materials and their configurations at the thin film interface. Interaction models have been developed to explain the experimental findings, but these dipole formation mechanisms with dipolar interface materials and the resulting energy level alignment have not been well established. For example, the direction and magnitude of the dipole moment of dipolar interface materials and the resulting device characteristics cannot be explained clearly without invoking the concept of decoupled dipoles (*e.g.* surface dipole, interface dipole and intrinsic dipoles) and considering further intramolecular or intermolecular interactions in the materials (*e.g.* depolarization effect and ion redistribution).[2–4] However the dipole moments of dipolar interface materials have been confused or misunderstood in previous reports of organic and perovskite solar cells.

In this review, we focus on clarifying the working mechanisms of diverse dipolar interface materials in organic and hybrid perovskite solar cells. We clearly show this by connecting theoretical and experimental findings. The mechanism by which the arrangement of dipolar molecules in the interface layer affects the resulting dipole moment at the interface is evaluated by using spontaneously or nonspontaneously aligned dipolar molecules (Fig. 1) to understand the decoupled dipole moment and the depolarization induced by neighbouring polar molecules. The decoupled interface dipole moments may contribute to determine the work function Φ of electrodes and the energy level alignment at the interface of devices. In addition, the decoupled interface dipole moment is strongly correlated with functionality, polarity, thickness of layer, and externally-applied electric field within the dipolar materials of interface layer. Furthermore, several experimentally-determined characteristics in organic and perovskite solar cells with dipolar interface materials are analysed to support this interface dipole moment mechanism.

Tae-Woo Lee

Tae-Woo Lee is an associate professor in Materials Science and Engineering at Seoul National University, Korea. He received his PhD in Chemical Engineering from KAIST, Korea in 2002. He joined Bell Laboratories, USA as a post-doctoral researcher and worked in Samsung Advanced Institute of Technology as a member of research staff (2003–2008). He was an associate professor in Materials Science and Engineering at Pohang University of Science and Technology (POSTECH), Korea until Aug, 2016. His research focuses on printed electronics based on organic and organic–inorganic hybrid materials for flexible displays, solid-state lightings, and solar-energy-conversion devices.

Interface dipole moments of dipolar interface materials

A. Introduction of decoupled interface dipole moment

Interface dipole moments are introduced to explain diverse effects of dipolar interface materials in organic and hybrid perovskite solar cells and clarify working mechanisms of localized dipole moment (Fig. 2). To understand alignment of interface dipole moment, spontaneously aligned dipolar interface molecules are investigated. Self-assembled monolayers (SAMs) of dipolar molecules are densely-packed and well-ordered two-dimensional dipolar organic molecules on a surface; SAMs have been used as a multi-functional interfacial layer to modify the macroscopic surface properties[7,8] and the effective Φ at interfaces.[9] In the field of thin-film electronics (*e.g.*, organic solar cells, perovskite solar cells, organic thin-film transistors, organic light emitting devices), SAMs have been employed for several critical functions, such as modifying gate dielectrics,[10–15] developing new device functionalities,[16,17] controlling the ordering and morphology of the organic semiconductor,[18,19] and improving charge carrier transfer.[18–24] Particularly SAMs have been selectively used to study localized dipole depending on diverse molecular conformations and configurations because SAM attach covalently and align to the substrate (Fig. 1a), so SAM's molecular arrangement has a clear relationship with the resulting dipole moment at the interface.[25]

SAMs can be seen as molecules composed of three parts: the docking group on the electrode, the backbone, and functional head-group facing organic layer (Fig. 2 upper). Density functional theory (DFT) calculations suggest that the dipoles at each end of the SAM (docking group and head group) are electrostatically decoupled and depolarization phenomena are observed in dipolar interface materials.[25–28]

Depolarization effect has been reported in the SAMs on a metallic surface. In a densely packed SAM, mutual interactions between the neighbouring molecules in the SAM should be considered.[25–28] The intermolecular charge interaction in the

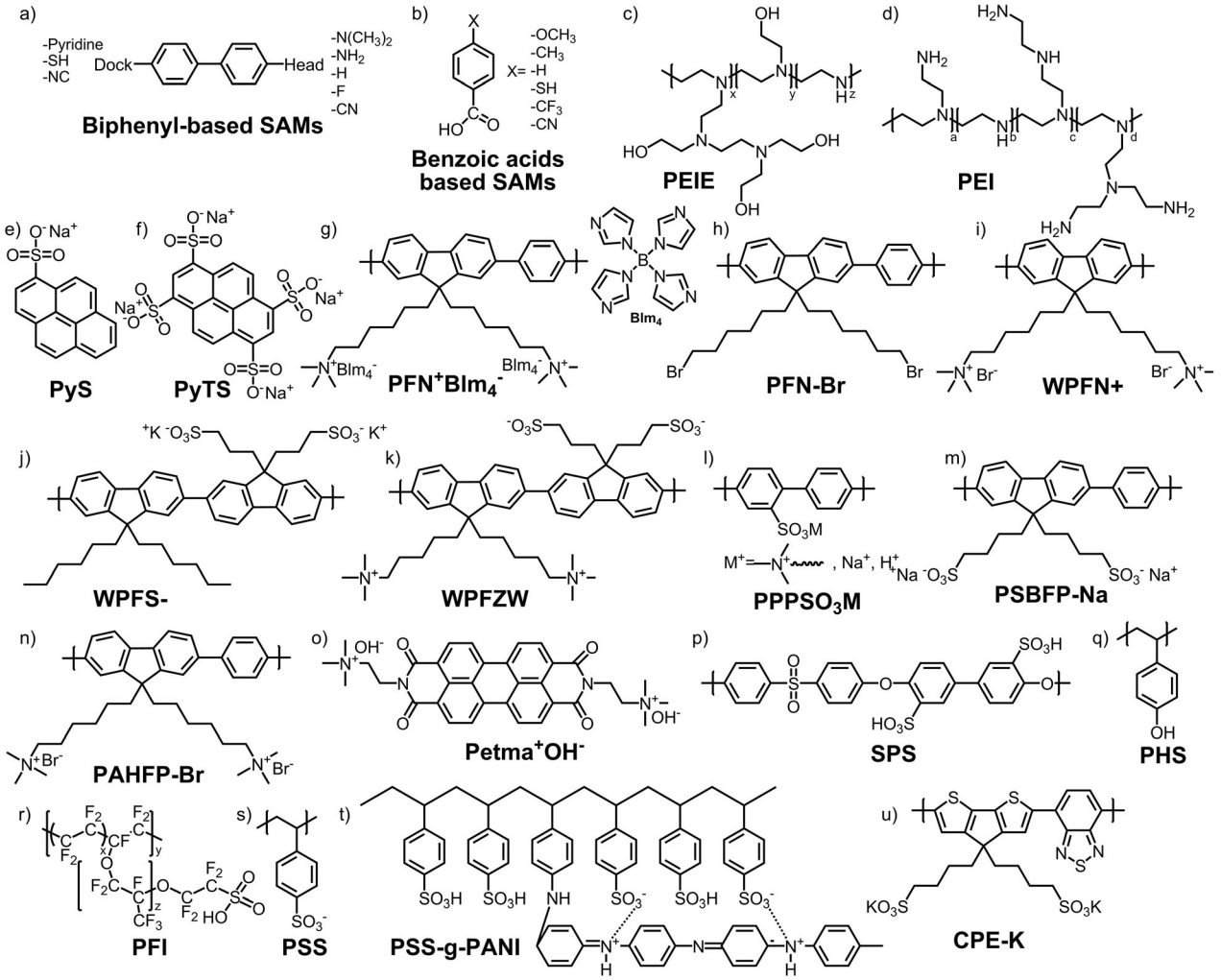

Fig. 1 Molecular structures of spontaneously or nonspontaneously aligned dipolar molecules. (a) Biphenyl-based SAMs,[25] (b) benzoic acids based SAMs,[34] (c) polyethylenimine ethoxylated (PEIE),[39] (d) branched polyethylenimine (PEI),[39] (e) 1-pyrenesulfonic acid sodium salt (PyS),[41] (f) 1,3,6,8-pyrenetetrasulfonic acid tetrasodium salt (PyTS),[41] (g) poly[9,9-bis[60-(*N*,*N*,*N*-trimethylammonium)-hexyl]fluorene-*alt*-*co*-1,4-phenylene]tetrakis (imidazoly)borate ($PFN^+Blm_4^-$),[42] (h) poly[9,9-bis(60-bromohexyl)fluorene-*alt*-*co*-1,4-phenylene] (PFN-Br),[42] (i) poly[9,9-bis(6′-(*N*,*N*,*N*-trimethylammonium)hexyl)fluorene]-bromide (WPFN+),[45] (j) potassium poly[9,9-bis(3′-sulfonatopropyl)fluorene-*alt*-(9,9-dihexylfluorene)] (WPFS−),[45] (k) potassium poly[9,9-bis[6′-(*N*,*N*,*N*-trimethylammonium)hexyl]-fluorene-*alt*-*co*-bis(3′-sulfonatopropyl)]bromide (WPFZW),[45] (l) sulfonated poly(*p*-phenylene) with ionogenic moieties ($PPPSO_3M$),[47] (m) poly[9,9′-bis(4-sulfonatobutyl)-fluorene-*alt*-1,4-phenylene]disodium salt (PSBFP-Na),[49] (n) poly[9,9′-bis(6″-*N*,*N*,*N*-trimethylammoniumhexyl]fluorene-*alt*-1,4-phenylene)dibromide (PAHFP-Br),[49] (o) perylene bis(2-ethyltrimethylammonium hydroxide imide) ($Petma^+OH^-$),[50] (p) sulfonated poly(phenylsulfone) (SPS),[52] (q) poly(4-hydroxystyrene) (PHS),[51] (r) perfluorinated ionomer (PFI),[55] (s) polystyrene sulfonate (PSS),[57] (t) poly(4-styrenesulfonate)-*g*-polyaniline (PSS-*g*-PANI),[58] (u) poly[2,6-(4,4-bis-potassiumbutanylsulfonate-4*H*-cyclopenta-[2,1-*b*;3,4-*b*′]-dithiophene)-*alt*-4,7-(2,1,3-benzothiadiazole)] (CPE-K).[60]

SAM induces the electric field which depolarizes individual molecules by inducing a dipole moment that opposes the intrinsic dipole moment μ_0 of a single isolated molecule and correspondingly, the dipole moment of each molecules is reduced by an effective dielectric constant ε_{eff} compared to μ_0 (Fig. 3).[29] Therefore, the dipole moment to the surface normal μ_z as

$$\mu_z = \mu_0 \cos\theta/\varepsilon_{\text{eff}}$$

where θ denotes the angle between the long molecular axes and the surface normal.[30–33] The fullerene with rigid pentapod-shape docking group that can form SAM with a constant θ was used to prove depolarization effect of dipolar interface materials quantitatively and corresponding energy level alignment.[28]

The interface dipole moments and corresponding electric field of end group could not penetrate to opposite side of layer, thereby each dipole moment at end groups of the SAM are independently decoupled. Therefore, no significant intramolecular charge transfer is found across the backbone of SAM molecules due to such dielectric screening. Work function modification $\Delta\Phi$ and energy level alignment are determined by each interface dipole moment of the docking group side and functional head-group side of SAM, not by μ_0. At the interface of docking side, the surface dipole by the electron cloud leaking out from

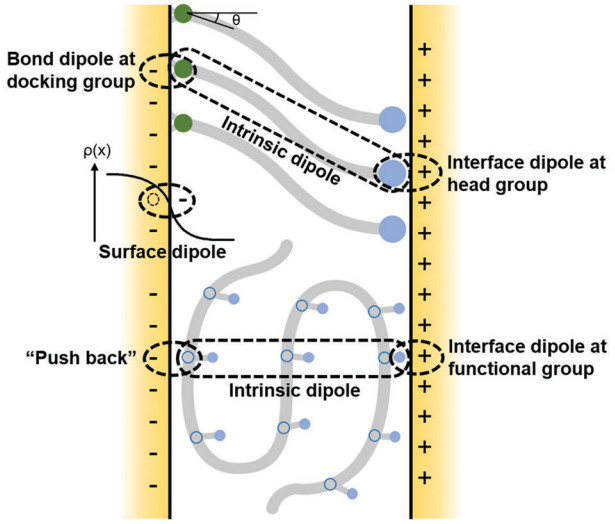

Fig. 2 Formation of diverse interface dipole moments which affect energy level alignment and the consequent device characteristics in organic and hybrid perovskite solar cells. Dipole moment of self-assembled monolayers (SAMs) is decoupled to have intrinsic dipole moment along backbone and interface dipole moments at docking group and head-group (upper). Dipole moment of a polar polymer is decoupled to have interface dipole and intrinsic dipole (below).

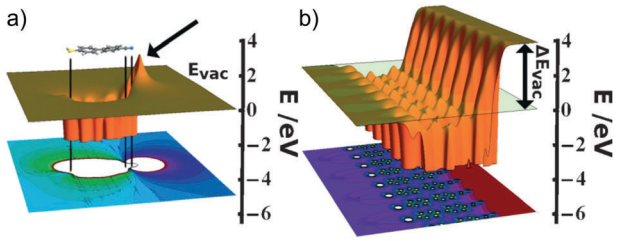

Fig. 3 Electron potential energy of (a) an isolated SAM molecule and (b) an infinitely-extended 2D SAM molecules averaged over one dimension. Black vertical lines: position of docking group and head group.[25] Reproduced from ref. 25 with permission from John Wiley and Sons.

metal substrate (Fig. 2 middle left) is attenuated by interface dipole moment of even weakly-adsorbed molecules, because the electrons are pushed back into the substrate (Fig. 4).[27] Bond formation and the resulting bond dipole (BD) between substrate and docking group of SAM shifts the entire potential distribution of the SAM.[2,3,27]

In the meantime, at the interface of head side, Φ and ionization energy (IE) are critically modified according to the potential step ΔU_{vac} created by the dipolar head-group (*e.g.*, cyano group, amino group) while remaining identical at the docking side regardless of the head-group molecule, because the interface dipole moment at head-group side does not affect the energy level alignment at the docking group side. For instance, Φ and IE at the interface of the head-group side are increased by cyano groups and decreased by amino groups, but the head group may not significantly influence the interface of the docking side. IE, ΔU_{vac}, and electron affinity (EA) at the docking side can change significantly depending on the

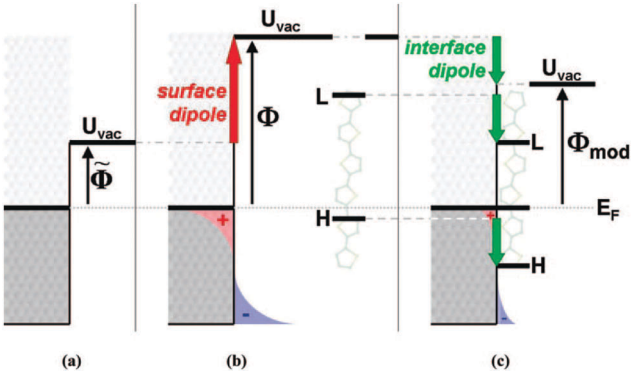

Fig. 4 Energy diagram with concepts of surface dipole and metal–molecule interface dipole. (a) Energy level of a metal surface, (b) a surface dipole moment at the metal surface raises vacuum level U_{vac} and increases the work function Φ (c) the electrons are pushed back into the metal by organic molecules, thereby the surface dipole is attenuated and work function is modified (Φ_{mod}).[27] Reproduced from ref. 27 with permission from American Chemical Society.

substituted group (Fig. 5).[25] Therefore, total $\Delta\Phi$ can be described as below.

$$\Delta\Phi = \Delta U_{vac} + BD$$

Φ is separately modified by decoupled interface dipole moments, and thus charge transfer energy offset is reduced in organic and hybrid perovskite solar cells.

B. Dipolar interface molecules in organic or hybrid perovskite solar cells

To quantify $\Delta\Phi$ contributed by dipolar interface materials in organic or hybrid perovskite solar cells, each decoupled interface dipole moment must be considered. Numerous interface materials[34–49] have been introduced and corresponding experimental characteristics are explained by the decoupled dipole moments and the depolarization induced by neighbouring polar molecules.

The interface dipole moment of SAM-modified ZnO/metal cathode interface affects the characteristics of organic solar cells.[33] A ZnO nanoparticle thin film on P3HT:PCBM layer was modified using carboxylic-acid-based SAM (Fig. 1b) having various head groups with different gas-phase dipole moment, $-OCH_3$ (−3.9D) < $-CH_3$ (−2.9D) < –H (−2.0D) < –SH (1.5D) < $-CF_3$ (2.1D) < –CN (3.7D). However the Schottky barrier at

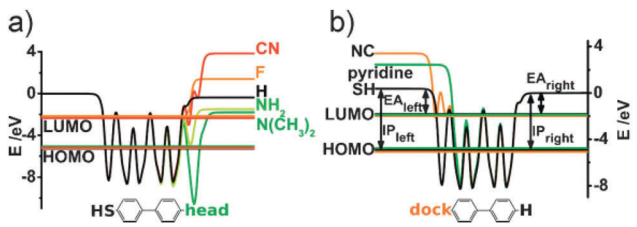

Fig. 5 Energy level shift of biphenyl-based SAMs depending on (a) the head groups and (b) the docking groups.[25] Reproduced from ref. 25 with permission from John Wiley and Sons.

ZnO/metal (*e.g.*, Al, Ag, Au) and device characteristics of organic solar cells with SAMs seem to contradict the predicted dipole moment, which is calculated using the intrinsic molecular dipoles. The intrinsic dipole moment was predicted to point toward metal from the ZnO surface in SAM with a head group of $-OCH_3$ and the corresponding Schottky barrier at ZnO/metal was expected to increase, however Schottky barrier at ZnO/metal was reduced by different dipole moment formed in a direction toward ZnO surface. This occurs because each end group of SAMs is decoupled and the intimate contact at the metal–molecule interface enables metal–molecule polarization, which causes the trend in interface dipole moment to be opposite to intrinsic dipole moment (Fig. 6). Therefore, the Schottky barrier at the SAM is strongly influenced by the net dipole moment, which is identical to interface dipole and has the opposite orientation with the intrinsic dipole moment.[34]

In hybrid perovskite solar cells as well as organic solar cells, the effect of dipolar interface molecules has been investigated. A 3-aminopropanioc acid (C_3-SAM) at ZnO/perovskite interface can modify Φ and improve the energy level alignment of $CH_3NH_3PbI_3$ perovskite solar cells.[35] The intrinsic dipole moment points from the ZnO substrate toward the perovskite layer due to the carboxylic-acid-based docking group and amino head group, so Φ of ZnO measured by UPS decreases from 4.17 to 3.52 eV with C_3-SAM. In the perovskite solar cell with C_3-SAM, the net dipole moment of ZnO/C_3-SAM/perovskite is determined along the intrinsic dipole moment (which points toward the ZnO layer) while the dipole moment of ZnO/SAM/metal is determined along interface dipole moment in ref. 35 and 36 (which points toward the metal layer). It is because dipole is not decoupled at the intimate contact between the SAM head group and free surface or organic interface whereas it is decoupled at the metal–molecule interface (Fig. 6).

Non-conjugated small-molecule electrolytes containing zwitterionic molecules that have a positive and a negative electrical charge, can be also used as an efficient interface layer.[37,38] The electrolytes are used as an electron extraction layer on top of the photoactive layer (conventional structure) or ZnO layer (inverted structure) in organic solar cells.[37] The effect of methanol treatment at the interface was additionally investigated to compare with the use of the electrolyte interlayer, because these electrolyte interlayers are dissolved in alcohol and formed on the substrate by spin-casting. In the conventional structure, methanol treatment increases the surface potential of the photoactive layer and open circuit voltage V_{oc} more than does treatment with electrolyte. However, the electrolyte-based devices have higher short circuit current density J_{sc} than the devices treated with methanol. In the inverted structure, devices with electrolyte on ZnO layer have higher J_{sc} than devices with methanol and without treatment, whereas the devices have identical V_{oc}. These differences in responses of J_{sc} and V_{oc} occur because J_{sc} and FF are increased by the enhanced charge extraction and the reduced charge recombination that are caused by the interface dipole moment of this non-conjugated small-molecule electrolyte contacted with (semi)conducting materials, whereas V_{oc} is increased by the high surface potential and the reduced number of surface defects on the ZnO film after methanol treatment. The electronic structure of electrolytes caused more balanced charge extraction and reduced recombination compared to the methanol treatment in both conventional and inverted organic solar cells due to interface dipole moment.[37]

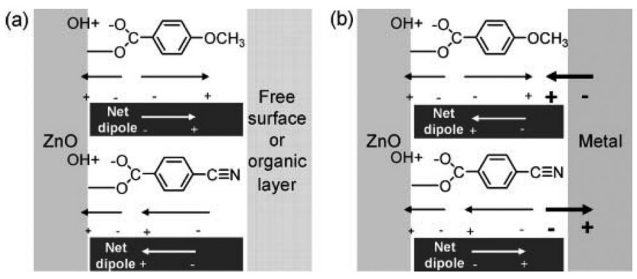

Fig. 6 Schematics for the interfacial dipole moments and net dipole moment between (a) a ZnO/SAM/free surface or organic layer, and (b) ZnO/SAM/metal junctions.[34] Reproduced from ref. 34 with permission from John Wiley and Sons.

The mechanism that leads to $\Delta\Phi$ of a polymeric interface material with insulating backbone and aliphatic amine groups, *i.e.* PEIE and PEI (Fig. 1c and d), can be determined by decoupling the interface dipole moment from intrinsic dipole moment.[39] An ultrathin (1 to 10 nm) layer of PEIE or PEI that is physisorbed on the surface of conducting materials (*e.g.*, metal, conductive metal oxide, conducting polymer, graphene) reduces Φ of conductors as electron-selective electrodes in organic solar cells. Although PEIE seems to be as an insulator (bandgap of 6.2 eV and non-conjugated backbone), but electrons can be extracted efficiently through PEIE interfacial layer due to $\Delta\Phi$ at the interface.[39]

When the pH values of the PEIE solution is adjusted ($4.5 \leq pH \leq 13$) to affect the degree of protonation of the amine groups in PEIE, Φ is primarily determined by the neutral amine groups in PEIE, not by protonated amine groups. This difference occurs because the neutral amine groups contribute to form interface dipoles, so Φ is modified (Fig. 7). To understand the possible mechanism, an ethylamine based SAM and ZnO substrates were considered in DFT calculation. The intrinsic dipole moment of the SAM towards the surface by an electrostatic potential energy change, and the interface dipole moment between SAM and ZnO reorient to toward the surface. As a result, the intrinsic dipole and the interface dipole contribute to modify Φ.[39]

PEIE can be used as an electron extraction layer between PCBM and metal electrode for highly efficient hybrid planar hetero-junction $CH_3NH_3PbI_{3-x}Cl_x$ perovskite solar cells.[40] As identically demonstrated in organic solar cells, Φ of the metal electrode (Ag) is reduced and PCE of the perovskite solar cells increases when a PEIE interfacial layer is used. The reduction in Φ may occur because by the interface dipole moment of PEIE, which induces the push-back effect at the metal interface to reduce surface dipole which causes a potential offset at the interface due to the electron cloud leaking out from metal substrate and the resulting dipole moment pointing toward

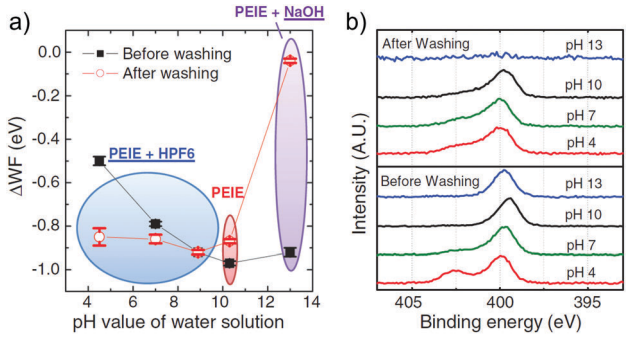

Fig. 7 (a) Work function modification of PEIE film on ITO depending pH values of solution. (b) X-ray photoelectron spectroscopy (XPS) to observe the degree of PEIE protonation.[39] Reproduced from ref. 39 with permission from the American Association for the Advancement of Science.

metal surface.[40] Although dipole moments of the PEIE interlayers in ref. 38 and 39 were orientated in the opposite directions (toward substrate surface and the air, respectively), this difference is also explained well by the theoretically demonstrated mechanism, which is that the interfacial dipole moment points out of the conductor to interlayer at the conductor/PEIE or PEIE/conductor interface.

Conjugated small-molecule electrolytes containing a number of anions directly linking to a conjugated core can be used to show the influence of intramolecular dipole moment and interface dipole moment of interface materials on the device performance.[41] Conjugated small-molecules with the pyrene as conjugated core substituted by one (PyS) and four (PyTS) anion groups (sodium sulfonate) (Fig. 1e and f) were used as interlayer materials in organic solar cells. Due to a large permanent dipole moment of PyS (4.85 debye), the Φ of photoactive layer was reduced and device characteristics were significantly enhanced in the organic solar cells with the PyS cathodic interlayer. In the other hand, overall dipole moment of PyTS is 0 debye due to the symmetrical arrangement of anions, so the Φ of photoactive layer was not changed with PyTS interlayer. However, the PyTS interlayer induced the interface dipole formation at the interface with cathode and therefore the device characteristics were noticeably enhanced compared to the device without interlayer or MeOH treatment. Even the Φ of photoactive layer was slightly reduced by MeOH treatment, the device with PyTS interlayer has higher PCE and carrier mobilities than that with MeOH treatment. Therefore, the interface dipole moment at the intimate contact with interface layer and conductor could be particularly effective as well as intramolecular dipole moment to enhance the device characteristics in organic solar cells.

C. Distribution and redistribution of interface dipole moments in conjugated polyelectrolytes

Polyelectrolyte refers to a macromolecule that include a large portion of the constitutional repeating units having ionisable, water-soluble, or ionic groups. The electrolytes in the repeating units of polyelectrolytes are covalently bonded to a backbone.[42] Ionomer, meanwhile, is a ion-containing macromolecule in which a smaller proportion of the units have ionisable or ionic groups.[42] Most of Ionomers have the repeating units of both non-polar (neutral) and ionized segments in a backbone. The ionomer can form small ionic clusters due to the phase separation of polar and non-polar segments.

Conjugated polyelectrolytes (CPEs) have been used as the charge extraction layer in organic and organic–inorganic hybrid perovskite solar cells to modify Φ of the electrode and to reduce the Schottky barrier.[43–50] CPEs are semiconductors and dissolved in polar solvents (*e.g.*, water, alcohol), and therefore can be cast in a thicker layer than the quantum mechanical tunnelling limit ($\sim$10 nm) underneath or atop the photoactive layer or electrode for efficient charge extraction. $\Delta\Phi$ of the CPE layer is also affected by the decoupled dipole moment (Fig. 2 below), which is strongly correlated with the degree of functionalities, polarities, and thickness of in CPEs.

The electronic structures of neutral and polar conjugated polymer deposited on a metal surface were investigated.[42] The polymers had a backbone of fluorine and phenylene copolymer, and different side chains (*i.e.*, neutral Br, N^+–Br^-, N^+–BIm_4^-, SO_3^-–Na^+) (Fig. 1g and h). Analyses by UPS and XPS showed strong band bending by the downward vacuum level shift in cationic CPEs (N^+–Br^- and N^+–BIm_4^-), but not in others (neutral Br, SO_3^-–Na^+) due to dipole free surface or less interfacial dipole. Moreover, the large counterion BIm_4^- (diameter $\sim$8.98 Å) led to larger dipole and band bending than Br^- ($\sim$3.92 Å) did.[43] In the same manner, when the CPEs with polyviologen backbone and various sizes of counterions (*i.e.*, Br^-, BF_4^-, $C_{24}H_{20}B^-$) were coated atop the photoactive layer, larger interfacial dipole and smaller $\Delta\Phi$ were obtained with increasing the size of counterions.[42] Furthermore, when CPEs with polyfluorene backbone and different polarities of counterions (*i.e.*, NH_4^+–Br^- side chain, SO_3^-–K^+ side chains, or both) (Fig. 1i–k) were placed on top of an ITO electrode, the dipole moment and $\Delta\Phi$ changed regarding to the polarities of counterions.[45] The cationic CPE with NH_4^+–Br^- side chain reduced Φ of ITO (0.43 eV), whereas the anionic CPE with SO_3^-–K^+ side chain increased Φ of ITO (0.25 eV). In addition, to investigate the dipole moment formation of CPE depending on functionalities, CPEs with a different number of side chain (N^+–Br^-) and different layer thickness were introduced.[45] CPE interlayers decrease the energy offset at cathode interface and increase device performance with increasing the number of side chains (from two to six in a repeat unit), because interface dipole moment of CPE increases with increasing ionic functionality. The high-performance organic solar cell is obtained when the thickness of the CPE layer is decreased (maximum PCE with 2 nm-thick CPE layer), because when the CPE layer is thinner than quantum mechanical tunnelling limit (3–5 nm), interfacial dipole is a dominant factor which modifies Φ of the CPE layer.[45]

Despite the promising properties and various uses of CPE charge extraction layer in organic and hybrid perovskite solar cells, in-depth mechanism of the net dipole moment and energy level adjustment at the interface is not fully understood because the molecular and dipolar orientations of CPEs are unclear unlike SAMs assembled by the nature of chemical bonding.

To understand what determines the net dipole moment and energy level adjustment at the interface, the molecular orientation and decoupled interface dipole moments of CPEs must be determined.

The redistribution of ionic groups in a CPE film, and the interface dipole moment were studied to understand the dipole formation in CPE interface layers and improve the energy level alignment. The ionic motion in the CPE film (Fig. 1l) was inspected in early studies of polyelectrolyte device with ITO/anionic CPEs/ITO structure. Under applied bias, the cationic counterions (Na^+ or H^+) are mobile whereas the negatively-charged group (SO_3^-) is fixed to the polymer backbone. Thus, the cations diffuse toward the negative electrode (cathode), so the anionic layer is formed close to the positive layer (anode); therefore, the space-charge profile is asymmetric (Fig. 8), and the potential drop across this anion concentrated layer is insufficient to compensate for the potential difference between the poly(*p*-phenylene)s (PPP) LUMO position and the Φ of ITO. As a consequence, the electroluminescence (EL) of this device is unstable over time.[47]

The redistribution of the counterions was later observed in the PLED device with a cationic CPE as an electron transporting layer (Fig. 1g). Because of ion motion, the time responses of current density J and luminance L were delayed by a few seconds depending on applied bias and the thickness of the cationic CPE interlayer. Normally the EL response of PLED occurs within nanoseconds or microseconds. In addition, the steady state J and L of devices decreased by the cationic CPE layer. This time response and drop of J and L at steady state in the device with CPE interlayer gradually decreased as the applied bias was increased (max 6 V) and as the thickness of the CPE layer was decreased (min 10 nm). It is because the electron injection barrier is reduced and corresponding electrical characteristics of the devices are improved as ion motion increases.[48]

In organic solar cells, ion motion of CPEs with polyfluorene backbone and opposite polarities of counterions (*i.e.*, NH_4^+–Br^- side chain, SO_3^-–Na^+ side chains) was investigated (Fig. 1m and n). The dipole reorientation and the resulting energy level adjustment were observed depending on the electric field to the device; this process is called as electric poling. When positive electric poling was applied to a device with a cation CPE interfacial layer, the anion counterions (Br^-) are redistributed toward the photoactive layer by the electrostatic force. As a result of this redistribution, Φ of the organic photoactive layer with the cation CPE interlayer is changed from −0.15 eV to +0.14 eV relative to Φ of the organic photoactive layer without the CPE interlayer. This dipole rearrangement suggests that the net dipole moment and $\Delta\Phi$ are determined primarily by the interface dipole moment of CPE at the intimate contact with the adjacent layer, *e.g.*, metal electrode or photoactive layer, not by the intrinsic dipole moment of CPE (Fig. 9). Therefore, after positive electric poling on anionic and cationic CPEs, the magnitudes of the interface dipole moments of CPE interlayers on the photoactive layer were nearly identical. In spite of the opposite functionality of anionic and cationic CPEs, the charged counterions are redistributed and aligned along the electric field.[49]

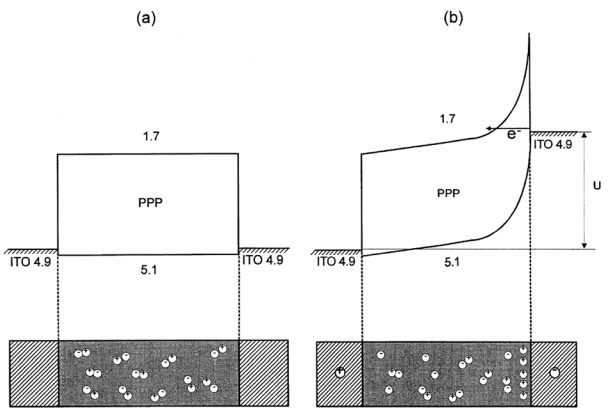

Fig. 8 Schematic energy level diagram for ITO/PPP based cation CPE/ITO device (a) without and (b) with an applied bias larger than the HOMO–LUMO separation of PPP.[47] Reproduced from ref. 47 with permission from John Wiley and Sons.

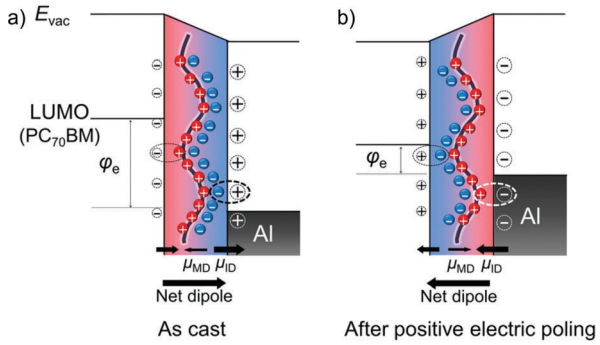

Fig. 9 Schematics of energy level alignment of the cationic CPE interlayer on the photoactive layer. Net dipoles for CPE interlayer are determined by interface dipole (a) toward metal electrode as cast and (b) toward photoactive layer after positive electric poling.[49] Reproduced from ref. 49 with permission from John Wiley and Sons.

The redistribution of mobile counterions in conjugated interlayer materials also can increase the intrinsic conductivity significantly. A perylene diimide (PDI) based $Petma^+OH^-$ (Fig. 1o) is soluble in water and becomes self-doped (n-type) by dehydration and then reversibly de-doped by hydration. After heating (120 °C, 20 min) the film, the $Petma^+OH^-$ molecules are dehydrated and transformed to PDI anions, then the Fermi level of that with the dehydrated state is nearly close to the conduction band edge. As a consequence of this transformation, Φ is decreased from 4.70 eV to 3.96 eV and the conductivity increased by ~5 orders of magnitude. However this self-doped PDI anion returns to de-doped state after a few days under humid air. Because of the reduced Φ and increased conductivity, the dehydrated and doped PDI anion is used as an efficient electron extraction layer in organic solar cells.[50]

D. Energy level alignment of dipolar interface layer

Polyelectrolyte with sub-monolayer thickness has been used for contact doping at the interface of ITO/photoactive layer in organic solar cells (Fig. 1p and q).[51,52] Compared to small-molecule dopants, the polyelectrolyte dopant are not prone to diffuse or

migrate into the intimate layer, therefore interface dipole is created by interfacial doping effect. As a result, the electrical characteristics of the device is enhanced with contact doping by a polyelectrolyte dopant. However this contact doping is critically affected by the thickness of the contact dopant layer. When the thickness of the polyelectrolyte dopant increases, charge carriers are blocked due to the insulating nature of the nonconjugated polyelectrolyte. Meanwhile, a thinner spin-cast polyelectrolyte layer (<3 nm measured by ellipsometry) than quantum mechanical tunnelling limit (3–5 nm) shows incomplete coverage on ITO substrate, thereby regions with and without contact dopant coexist on the device.[52]

To observe the coverage effect of sub-monolayer thick dipolar interlayer on energy level alignment at the interface, an ultrathin metal fluoride layer at the interface of P3HT:PCBM/Al was studied. BaF_2 was deposited by thermal evaporation on the P3HT:PCBM surface, then thermodynamically redistributed to increase its grain size (island-growth mode); therefore ultrathin BaF_2 layers that were thinner than a monolayer (~3 nm) partially cover the surface of the underneath layer. Because of this partial coverage by the BaF_2 layer, the degree of dipole moment gradually increased until a completed monolayer is formed. Therefore, despite the insulating nature of BaF_2, the device characteristics such as V_{oc}, J_{sc}, and FF in organic solar cells are improved due to the increased built-in potential and the decreased series resistance R_s. However, a BaF_2 interlayer thicker than a monolayer shows a charge blocking property.[53] Similarly, a 1 nm-thick LiF interlayer has been used in planar p–i–n perovskite solar cells. A LiF interlayer thinner than monolayer creates Ohmic contact between n-type PCBM layer and Al electrode due to the formation of a dipole moment; therefore R_s is significantly reduced.[54]

Even though a strong dipole moment of nonconjugated polyelectrolytes is formed at the interface and modifies $\Delta\Phi$, they have an insulating nature, so they are useful only if their thickness is less than monolayer.[52] Fluorinated ionomer (Fig. 1r) is used as a strong dopant molecule and mixed with a conducting polymer to be used as an efficient hole extraction layer in organic or hybrid perovskite solar cells.[55,56] This fluorinated ionomer has high IE and low surface energy, and thus forms a self-organized polymeric dopant layer enriched at surface. $\Delta\Phi$ of fluorinated ionomer-blended conducting polymer is increased according to the molecular doping ratio.[55] The conductivity of fluorinated ionomer-blended film is comparable to that of untreated film. Consequently, the energy level of the conducting polymer can be systematically tailored by adjusting the mixing ratio of the fluorinated ionomer to control the energy level offset with the photoactive materials of diverse highest occupied molecular orbital (HOMO) or valence band maximum (VBM) levels (Fig. 10).[55,56]

In UPS measurement, the Fermi level of the conducting polymer blend is pinned at an energy states of photoactive materials that are 0.4–0.7 eV shallower than the HOMO (or VBM) levels, *i.e.*, midgap state or bipolaron state. In contrast, the fluorinated ionomer suppresses and reduces the density of states of the conducting polymer in which it is mixed, so the interfacial

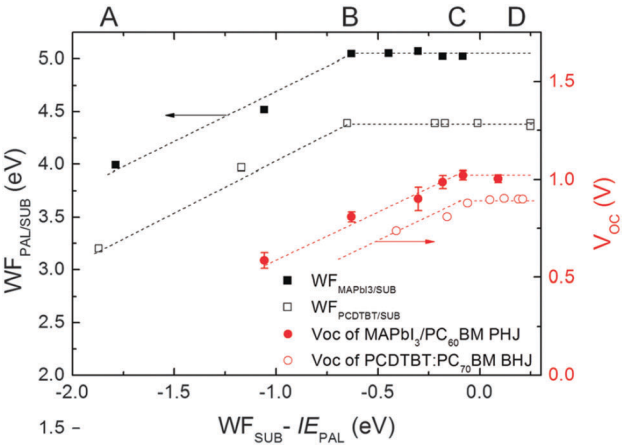

Fig. 10 Open circuit voltage and the work function of the perovskite ($CH_3NH_3PbI_3$ ($MAPbI_3$)/$PC_{60}BM$) (filled) and the organic (PCDTBT:$PC_{70}BM$) (open) solar cells depending on the difference of the conducting substrate work function (WF_{SUB}) and ionization energy of the photoactive layer (IE_{PAL}).[55]

energy state is created below the Fermi level and is aligned to the HOMO (or VBM) level of photoactive materials for ohmic contact at the interface. Even though the Fermi level is pinned at the midgap state of the photoactive layer, the electrons at the midgap state of the photoactive material are transferred across to the interface energy state of the hole extraction material until equilibrium is achieved. Therefore, a charge-transfer-induced interfacial dipole moment is observed at the equilibrated interface as evidence of ohmic contact.[55]

Despite the numerous advantages of polymeric hole extraction layers, the dopant-mixed conducting polymers (*e.g.*, PEDOT:PSS) have limited Φ that originates from the ratio of dopant molecules (*e.g.*, PSS (Fig. 1s)).[57] A self-doped conducting polymer is used as an efficient hole-extraction layer in hybrid perovskite solar cells. A PSS grafted polyaniline (PSS-*g*-PANI) is used as a hole-extraction layer for better energy level alignment with VBM of $CH_3NH_3PbI_3$ perovskite. The interface energy state of the PSS-*g*-PANI layer is modified (0.19 eV larger than PEDOT:PSS) by controlling the molecular ratio of PSS to PANI, therefore higher efficiency is achieved in the device with PSS-*g*-PANI (Fig. 1t) interlayer compared to that with PEDOT:PSS. Conventionally, polyelectrolyte acid-dopant mixed conducting polymer films are formed from the polymer-dispersed acidic solution and the aggregation of the molecules can occur when the conducting polymers are de-doped by change of environmental condition. These aggregated molecules might act as the serious defects in the device. However, in the case of self-doped conducting copolymer, the polyelectrolyte acid dopant is attached to the conducting backbone by covalent bonding, so this copolymer is solvated in water solution and the uniform layer can be formed without aggregation. Therefore, it shows low bimolecular recombination in the device.[58]

CPEs with self-doping effects occurring in the backbone have also been introduced as efficient hole extraction layers in organic and perovskite solar cells (Fig. 1u).[59,60] The self-doping process in the CPEs can occur due to the formation of polarons in the backbone of CPEs and the following stabilization by the pendent

sulfonate groups.[62] CPEs with smaller counterions compared to tetrabutylammonium, and shorter side chains have high doping levels, so the CPE with K^+ ion and short alkyl side chain (3.7–3.8 Å) has relatively high conductivity.[61] In addition, using the self-doped CPEs as a hole extraction layer is advantageous in terms of stability because they are chemically dissolved in the water/methanol solvent and pH neutral, whereas the conventional PEDOT:PSS is the mechanically mixed solution of a conducting polymer and dopant polyelectrolyte acid. Therefore the interfacial interaction with the photoactive materials containing Lewis base molecules is minimized with the pH neutral CPE interlayer.[59] In addition, the self-doped CPEs is stable in solution over time and in a wide range of pH of the solution, which lead to excellent film forming property. The self-doped CPE layer showed fewer surface defects at the film surface.[58]

Conclusions

We have reviewed current understanding of the decoupled dipole moments at the interface, and consequent energy alignment of dipolar interface materials. We make four observations. (1) The relationship between molecular arrangement and the consequent dipole arrangement has been inspected using self-assembled monolayers (SAMs) and conjugated polyelectrolytes (CPEs) to reveal the decoupled and depolarized dipole moment based on the controlled molecular configuration. (2) The decoupled interface dipoles (*e.g.*, bond dipole, intrinsic dipole, interface dipole of functional group) affect $\Delta\Phi$ and the energy level alignment in the device. (3) The decoupled dipole moment, particularly interface dipole moment, is strongly correlated with the functionality, polarity, thickness of layer, and externally applied electric field within the dipolar interface materials. (4) Several experimental characteristics in organic and hybrid perovskite solar cells with diverse dipolar interface materials demonstrate the working mechanism of the interface dipole moment.

Consequently the energy level alignment at the interface of the diverse dipolar interface materials, *e.g.*, self-assembled monolayers, conjugated or nonconjugated polymer, neutral molecules or electrolytes, zwitterion based molecules, electrolyte grafted copolymer, is clearly demonstrated and classified in terms of concrete concepts in organic and hybrid perovskite solar cells, *e.g.*, surface dipole, interface dipole, bond dipole, intrinsic dipole, rearranged dipole by ion redistribution, dipole by diverse molecular conformations and configurations, and self-doping effect with dipolar molecule. We conclude that energy level alignment at the interface can be clearly understood and developed by studying the mechanisms of the decoupled interface dipole moments, then the device characteristics of organic and hybrid perovskite solar cells are meaningfully enhanced by the insights provided in this review. As the designing principles for the effective interface materials, the composition, configuration, conformation, and arrangement of interface materials should be simultaneously considered for the direction and magnitude of intramolecular intrinsic dipole moment and also decoupled dipole moment at intimate contact with adjacent layers.

Conflicts of interest

There are no conflicts to declare.

Acknowledgements

This work was supported by the National Research Foundation of Korea (NRF) grant funded by the Korea government (MSIT) (NRF-2016R1A3B1908431).

Notes and references

1 H. Kim, K.-G. Lim and T.-W. Lee, *Energy Environ. Sci.*, 2016, **9**, 12.
2 H. Ishii, K. Sugiyama, E. Ito and K. Seki, *Adv. Mater.*, 1999, **11**, 605.
3 S. Braun, W. R. Salaneck and M. Fahlman, *Adv. Mater.*, 2009, **21**, 1450.
4 A. Kahn, N. Koch and W. Y. Gao, *J. Polym. Sci., Part B: Polym. Phys.*, 2003, **41**, 2529.
5 P. Broms, J. Birgersson, N. Johansson, M. Logdlund and W. R. Salaneck, *Synth. Met.*, 1995, **74**, 179.
6 P. Broms, J. Birgerson and W. R. Salaneck, *Synth. Met.*, 1997, **88**, 255.
7 G. K. Jennings and P. E. Laibinis, *Colloids Surf., A*, 1996, **116**, 105.
8 J. Genzer and K. Efimenko, *Science*, 2000, **290**, 2130.
9 I. H. Campbell, S. Rubin, T. A. Zawodzinski, J. D. Kress, R. L. Martin, D. L. Smith, N. N. Barashkov and J. P. Ferraris, *Phys. Rev. B: Condens. Matter Mater. Phys.*, 1996, **54**, R14321.
10 P. Fontaine, D. Goguenheim, D. Deresmes, D. Vuillaume, M. Garet and F. Rondelez, *Appl. Phys. Lett.*, 1993, **62**, 2256.
11 A. Facchetti, M. H. Yoon and T. J. Marks, *Adv. Mater.*, 2005, **17**, 1705.
12 M.-H. Yoon, A. Facchetti and T. J. Marks, *Proc. Natl. Acad. Sci. U. S. A.*, 2005, **102**, 4678.
13 M. Halik, H. Klauk, U. Zschieschang, G. Schmid, C. Dehm, M. Schutz, S. Maisch, F. Effenberger, M. Brunnbauer and F. Stellacci, *Nature*, 2004, **431**, 963.
14 K. P. Pernstich, S. Haas, D. Oberhoff, C. Goldmann, D. J. Gundlach, B. Batlogg, A. N. Rashid and G. Schitter, *J. Appl. Phys.*, 2004, **96**, 6431.
15 S. Kobayashi, T. Nishikawa, T. Takenobu, S. Mori, T. Shimoda, T. Mitani, H. Shimotani, N. Yoshimoto, S. Ogawa and Y. Iwasa, *Nat. Mater.*, 2004, **3**, 317.
16 X. F. Guo, M. Myers, S. X. Xiao, M. Lefenfeld, R. Steiner, G. S. Tulevski, J. Y. Tang, J. Baumert, F. Leibfarth, J. T. Yardley, M. L. Steigerwald, P. Kim and C. Nuckolls, *Proc. Natl. Acad. Sci. U. S. A.*, 2006, **103**, 11452.
17 P. Pacher, A. Lex, V. Proschek, H. Etschmaier, E. Tchernychova, M. Sezen, U. Scherf, W. Grogger, G. Trimmel, C. Slugovc and E. Zojer, *Adv. Mater.*, 2008, **20**, 3143.
18 C. Bock, D. V. Pham, U. Kunze, D. Kafer, G. Witte and C. Woll, *J. Appl. Phys.*, 2006, **100**, 114517.
19 K. Ihm, B. Kim, T. H. Kang, K. J. Kim, M. H. Joo, T. H. Kim, S. S. Yoon and S. Chung, *Appl. Phys. Lett.*, 2006, **89**, 033504.

20 P. Marmont, N. Battaglini, P. Lang, G. Horowitz, J. Hwang, A. Kahn, C. Amato and P. Calas, *Org. Electron.*, 2008, **9**, 419.
21 B. H. Hamadani, D. A. Corley, J. W. Ciszek, J. M. Tour and D. Natelson, *Nano Lett.*, 2006, **6**, 1303.
22 I. H. Campbell, S. Rubin, T. A. Zawodzinski, J. D. Kress, R. L. Martin, D. L. Smith, N. N. Barashkov and J. P. Ferraris, *Phys. Rev. B: Condens. Matter Mater. Phys.*, 1996, **54**, R14321.
23 I. H. Campbell, J. D. Kress, R. L. Martin, D. L. Smith, N. N. Barashkov and J. P. Ferraris, *Appl. Phys. Lett.*, 1997, **71**, 3528.
24 B. de Boer, A. Hadipour, M. M. Mandoc, T. van Woudenbergh and P. W. M. Blom, *Adv. Mater.*, 2005, **17**, 621.
25 G. Heimel, F. Rissner and E. Zojer, *Adv. Mater.*, 2010, **22**, 2494.
26 G. Heimel, L. Romaner, J.-L. Bredas and E. Zojer, *Phys. Rev. Lett.*, 2006, **96**, 196806.
27 G. Heimel, L. Romaner, E. Zojer and J.-L. Bredas, *Acc. Chem. Res.*, 2008, **41**, 721–729.
28 S. Lacher, Y. Matsuo and E. Nakamura, *J. Am. Chem. Soc.*, 2011, **133**, 16997.
29 L. Romaner, G. Heimel, C. Ambrosch-Draxl and E. Zojer, *Adv. Funct. Mater.*, 2008, **18**, 3999.
30 T.-W. Lee, J. Zaumseil, S. H. Kim and J. W. P. Hsu, *Adv. Mater.*, 2004, **16**, 2040.
31 T.-W. Lee, O. O. Park, L.-M. Do, T. Zyung, T. Ahn and H.-K. Shim, *J. Appl. Phys.*, 2001, **90**, 2128.
32 C. Goh, S. R. Scully and M. D. McGehee, *J. Appl. Phys.*, 2007, **101**, 114503.
33 K.-G. Lim, M.-R. Choi and T.-W. Lee, *Mater. Today Energy*, 2017, **5**, 66.
34 H. L. Yip, S. K. Hau, N. S. Baek, H. Ma and A. K. Y. Jen, *Adv. Mater.*, 2008, **20**, 2376.
35 L. Zuo, Z. Gu, T. Ye, W. Fu, G. Wu, H. Li and H. Chen, *J. Am. Chem. Soc.*, 2015, **137**, 2674.
36 K. B. Wiberg, *J. Org. Chem.*, 2002, **67**, 4787.
37 Z. Liu, X. Ouyang, R. Peng, Y. Bai, D. Mi, W. Jiang, A. Facchetti and Z. Ge, *J. Mater. Chem. A*, 2016, **4**, 2530.
38 A. Salomon, D. Berkovich and D. Cahen, *Appl. Phys. Lett.*, 2003, **82**, 1051.
39 Y. Zhou, C. Fuentes-Hernandez, J. Shim, J. Meyer, A. J. Giordano, H. Li, P. Winget, T. Papadopoulos, H. Cheun, J. Kim, M. Fenoll, A. Dindar, W. Haske, E. Najafabadi, T. M. Khan, H. Sojoudi, S. Barlow, S. Graham, J.-L. Brédas, S. R. Marder, A. Kahn and B. Kippelen, *Science*, 2012, **336**, 327.
40 H. Zhang, H. Azimi, Y. Hou, T. Ameri, T. Przybilla, E. Spiecker, M. Kraft, U. Scherf and C. J. Brabec, *Chem. Mater.*, 2014, **26**, 5190.
41 L. Zhou, W. Yu, S. Yu, P. Fu, X. Guo and C. Li, *J. Mater. Chem. A*, 2017, **5**, 657.
42 A. D. Jenkins, P. Kratochvíl, R. F. T. Stepto and U. W. Suter, *Pure Appl. Chem.*, 1996, **68**, 2287.
43 J. H. Seo, R. Yang, J. Z. Brzezinski, B. Walker, G. C. Bazan and T. Q. Nguyen, *Adv. Mater.*, 2009, **21**, 1006.
44 T. T. Do, H. S. Hong, Y. E. Ha, J. Park, Y. C. Kang and J. H. Kim, *ACS Appl. Mater. Interfaces*, 2015, **7**, 3335.
45 R. Kang, S.-H. Oh and D.-Y. Kim, *ACS Appl. Mater. Interfaces*, 2014, **6**, 6227.
46 B. H. Lee, I. H. Jung, H. Y. Woo, H.-K. Shim, G. Kim and K. Lee, *Adv. Funct. Mater.*, 2014, **24**, 1100.
47 D. Neher, J. Gruner, V. Cimrova, W. Schmidt, R. Rulkens and U. Lauter, *Polym. Adv. Technol.*, 1998, **9**, 461.
48 C. Hoven, R. Yang, A. Garcia, A. J. Heeger, T. Q. Nguyen and G. C. Bazan, *J. Am. Chem. Soc.*, 2007, **129**, 10976.
49 K.-G. Lim, S. M. Park, H. Y. Woo and T.-W. Lee, *ChemSusChem*, 2015, **8**, 3062.
50 T. H. Reilly III, A. W. Hains, H.-Y. Chen and B. A. Gregg, *Adv. Energy Mater.*, 2012, **2**, 455.
51 K.-G. Lim, M.-R. Choi, H.-B. Kim, J. H. Park and T.-W. Lee, *J. Mater. Chem.*, 2012, **22**, 25148.
52 G. K. Mor, D. Jones, T. P. Le, Z. Shang, P. J. Weathers, M. K. B. Woltermann, K. Vakhshouri, B. P. Williams, S. A. Tohran, T. Saito, R. Verduzco, A. Salleo, M. A. Hickner and E. D. Gomez, *Adv. Energy Mater.*, 2014, 1400439.
53 K.-G. Lim, M.-R. Choi, J.-H. Kim, D. H. Kim, G. H. Jung, Y. Park, J.-L. Lee and T.-W. Lee, *ChemSusChem*, 2014, **7**, 1125.
54 X. Liu, H. Yu, L. Yan, Q. Dong, Q. Wan, Y. Zhou, B. Song and Y. Li, *ACS Appl. Mater. Interfaces*, 2015, **7**, 6230.
55 K.-G. Lim, S. Ahn, Y.-H. Kim, Y. Qi and T.-W. Lee, *Energy Environ. Sci.*, 2016, **9**, 932.
56 K.-G. Lim, H.-B. Kim, J. Jeong, H. Kim, J. Y. Kim and T.-W. Lee, *Adv. Mater.*, 2014, **26**, 6461.
57 D.-H. Kim, K.-G. Lim, J. H. Park and T.-W. Lee, *ChemSusChem*, 2012, **5**, 2053.
58 K.-G. Lim, S. Ahn, H. Kim, M.-R. Choi, D. H. Huh and T.-W. Lee, *Adv. Mater. Interfaces*, 2016, **3**, 1500678.
59 H. Zhou, Y. Zhang, C.-K. Mai, S. D. Collins, T.-Q. Nguyen, G. C. Bazan and A. J. Heeger, *Adv. Mater.*, 2014, **26**, 780.
60 H. Choi, C. K. Mai, H. B. Kim, J. Jeong, S. Song, G. C. Bazan, J. Y. Kim and Al. J. Heeger, *Nat. Commun.*, 2015, **6**, 7348.
61 C.-K. Mai, R. A. Schlitz, G. M. Su, D. Spitzer, X. Wang, S. L. Fronk, D. G. Cahill, M. L. Chabinyc and G. C. Bazan, *J. Am. Chem. Soc.*, 2014, **136**, 13478.
62 C.-K. Mai, H. Q. Zhou, Y. Zhang, Z. B. Henson, T.-Q. Nguyen, A. J. Heeger and G. C. Bazan, *Angew. Chem., Int. Ed.*, 2013, **52**, 12874.

